Steering and Horizontal Motion Control in Insect-Inspired Flapping-Wing MAVs: The Tunable Impedance Approach

Hosein Mahjoubi, and Katie Byl

***Abstract*—Inspired by insect flight, flapping-wing micro-aerial vehicles (FWMAVs) are an ongoing design problem, posing exceptional challenges in morphological construction, force production, and control methodology. Some impressive initial results have emerged from work focused on generating sufficient lift force for levitation or vertical acceleration [1]; however, effective methods for motion control remain an open problem. In this work, we propose and analyze a simplified approach to the FWMAV maneuvering problem that 1) focuses on motion control and steering in the horizontal plane and 2) employs a wing design that relies on tunable passive dynamics to set the angle of attack. Our simulated experiments with this method demonstrate an exceptional capability in handling pitch tracking and steering maneuvers, even in presence of measurement noise. We compare the performance of our approach with that of another promising technique for steering: the "*split cycle*" [2]. Simulation results suggest that in our approach, steering maneuvers and planar motion are both faster and smoother. Furthermore, a passive dynamic control approach in FWMAV proves to have considerably lower bandwidth requirements. We will discuss how this is advantageous when designing a real FWMAV.**

***Keywords*—Microrobotics; Aerial Robotics; Insect Flight; Tunable Impedance; Passive Dynamics; Maneuverability; Steering; Simulation.**

I. Introduction

Modern technological advances in miniaturization across a wide range of robotics technology, from sensing, actuation and microprocessor design to micro-fabrication techniques and battery technology are increasingly enabling the growing field of microrobotics – particularly the development of insect-scale flapping-wing robots. Although manmade design solutions for modes of microrobotic motion are often highly influenced by insect locomotion, much work remains in adapting general known physical laws for force production into practical control strategies for reliable motion.

In this paper, we investigate and compare two recently proposed approaches to insect-inspired FWMAV control. Both approaches employ a rotational (torsional) spring element to set the angle of attack of the wing as it moves through the air. This couples the wing pitch angle to the stroke angle, so that angle of attack is set only indirectly, i.e., passively, while the gross stroke angle of the wing back and forth is powered actively during flapping. In one approach, referred to throughout as the "split cycle" (SC) method [2], the spring properties are set at constant values for all time, and control forces and torques are generated by introducing asymmetries in the up- and down- strokes of flight. In the second approach, which we will call the "tunable impedance" (TI) method [3], the set point of the spring (ψ_0) is allowed to vary on a slow time scale, compared to the frequency of flapping while the stroke profile remains symmetric.

Issues we address in this paper include: How does each method quantifiably perform? And what principles may explain one performs "better"? Briefly, our simulations indicate that the TI approach should provide better tracking while also providing the benefit of lower bandwidth requirements both in actuator dynamics and the feedback control loop [3], overall. These results support development of novel design and manufacturing techniques to exploit tunable passive stiffness in FWMAVs.

Below, we conclude this introduction with some general background on the use of passive dynamics in locomotion and on the practical control limitations of both insects and robots designed for high-frequency flapping.

A. Passive Dynamics in Locomotion

Over the past two decades, robotics researchers have increasingly acknowledged the importance of passive dynamics in achieving natural-looking and energy-efficient motions, specifically in the field of legged robotics [4]-[6]. By selecting inertial properties (mass distribution) and kinematics of the legs appropriately, some of the dynamic of a near limit-cycle motion can be *intentionally coupled*, with the aim of reducing both complexity and power consumption of active control elements for locomotion. However, this passive coupling can potentially limit the level of controllability; to date, passive-based walking robots remain undesirably sensitive to rough terrain or other impulsive perturbations from a near limit-cycle gait.

More recently, a variety of researchers studying flapping-wing flight have explored the potential of passive principles in achieving appropriate wing motions for effective lift generation [7]-[9]. We anticipate that the use of passive dynamics in FWMAV design has potential upsides and pitfalls similar to those observed for passive-based walking robots.

H. Mahjoubi and K. Byl are with the Robotics Laboratory, Department of Electrical and Computer Engineering, University of California at Santa Barbara, Santa Barbara, CA 93106 USA (e-mail: h.mahjoubi@ece.ucsb.edu, katiebyl@ece.ucsb.edu).

Both FWMAVs and agile flying insects face similar problems in design, manufacture, and control. Stated broadly, in both cases the performance goals in motion control range from high maneuverability to perturbation-robust hovering, and practical solutions should minimize any additional onboard weight and complexity to the greatest extent possible. In short, one might anticipate that there is typically a trade-off to be made between good passive stability, which rejects external *perturbation* forces, and effective steering capabilities, which are sensitive to commanded variations in *control* forces.

B. Bio-Inspired Actuation Strategies

Many insects employ two types of muscles in flight: *synchronous* and *asynchronous*. Insects are the only animals known to use asynchronous muscle. Even more ancient aerobaticists in the insect world, including dragonflies "which are considered to be relatively primitive fliers" [10], employ *only* synchronous muscles, which power the wings directly. Asynchronous muscle is, by contrast, a relatively advanced design feature, in evolutionary terms. Generally speaking, asynchronous muscle has facilitated the evolution of smaller and much faster (up to 1000 Hz, for a small midge) agile flyers than can be found within the purely synchronous muscled group; a locust beats its wings at about 16 Hz, for example [10].

Asynchronous muscles are employed in a specialized actuation strategy that can achieve a very rapid, cyclical power stroke by exciting a resonant mechanical load in the body structure. In highly agile insects that use *both* types of muscle, including flies and bees, synchronous muscles, by contrast, operates not in establishing the cyclical power stroke but in influencing wing's pitch rotation and functions more subtly, primarily to generate steering forces rather than to drive the gross velocity of the wing [11].

Flies also embody a "remarkable economy of control" [12]. Despite significant coupling between the forces and torques generated to control the six degrees of freedom of the body, they achieve astonishingly agile flight [12].

In both insects and flapping-wing microrobots, one reason for employing two types of actuators is to divide functionality between a nearly invariant, limit-cycle power actuation (e.g., asynchronous muscle) and a set of more efficient steering actuators (synchronous muscle) that only need to vary with a bandwidth that is a fraction of the flapping frequency[1]. Such a divided strategy, employed by flies and bees, is analogous to the *tunable impedance* approach analyzed in this paper, while a purely stroke-based actuation strategy is analogous to the *split cycle* method.

A "divided" actuation strategy can provide obvious practical utilities in coping with the bandwidth limitations of traditional actuators, such as DC motors, which are better-suited to a constant-velocity rotation than to high bandwidth actuation. Although the piezo actuators employed in the notable Harvard microrobotic fly [1] are well-suited to high bandwidth motion, they also require substantial innovations in power electronics, to generate the high voltages required for an untethered robot.

Finally, we note that asynchronous muscle has apparently evolved through at least 6 independent evolutionary lines [10]. Given its apparent evolutionary efficacy, it is also interesting to inquire whether a divided actuator strategy affords an advantage in control authority, beyond the known gains in power efficiency. Our simulation results provide evidence that such potential does indeed exist.

The rest of the paper is organized as follows. Section II outlines a basic aerodynamic model along with the key ideas behind split cycle and tunable impedance methods. In Section III, the modeled MAV used in our simulations is described and Section IV reviews the details of the controllers developed for motion control. In Section V, we present the results, and finally, Section VI concludes the paper.

II. Preliminary Considerations

The wing rotation model used in this work is based on a passive dynamic approach proposed by Byl [9]. In this approach, the wings are driven actively via a simple, sinusoidal power stroke while the angle of attack of each wing is adjusted passively throughout the stroke, as dictated by its mechanical impedance properties. Assuming that the inertia of the wing is small, the aerodynamic pitch torque (τ_ψ) should be in balance with the torque produced by torsional stiffness (τ_k) due to wing's pitch rotation (ψ) from its equilibrium angle ψ_0 (Fig. 1.a):

$$\tau_\psi = z_{CoP}\ F_N \tag{1}$$

$$\tau_k = k\ (\psi - \psi_0) \tag{2}$$

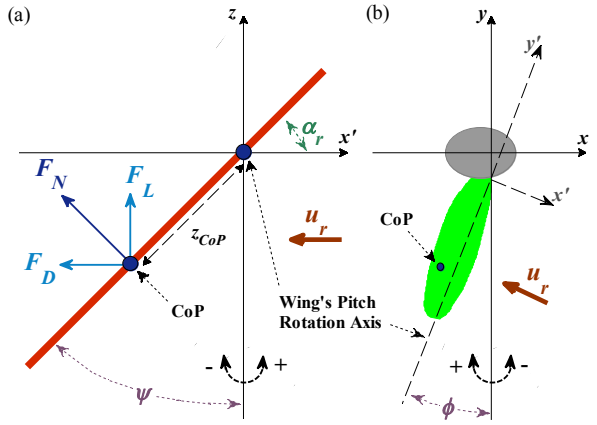

Fig. 1. (a) Wing cross-section (in downstroke) at CoP, illustrating the pitch angle of the wing ψ and orientation of aerodynamic forces. Note that in this case, the produced drag force F_D is negative. (b) Overhead view of the wing/body setup which defines the stroke angle ϕ.

[1] That is, it will take several wingbeats to accomplish a single maneuver.

$$\tau_{\psi} = \tau_{k} \tag{3}$$

where F_N is the aerodynamic force normal to the surface of the wing and z_{CoP} represents the distance of center of pressure (CoP) on the wing from the wing's pitch rotation axis (Fig. 1.a). k and ψ_0 are the impedance properties of joint's passive structure [9] (i.e. stiffness and set point) and they can be adjusted at a relatively slow rate, e.g., by changing the tensions in an opposing pair of tendons [13] along each wing. The value of k can be optimized to attain the maximum amount of lift force possible [9], and in this work, it is set to the lift-optimizing value of $k = 1.03\times10^{-6}$ (N.m/rad) for a sinusoid stroke profile of magnitude 35° at 100 Hz.

The wing shape we use here is the same as in [9] with its span set to 15 mm which results in z_{CoP} = 1.009 mm. For such a small wing flapping at 100 Hz, the Reynolds number is low enough (~3,000) to assume that the flow across the wing is quasi-stationary. This assumption enables us to use Blade Element Method (BEM) [14]-[15] to derive a first-order estimate of the dominant components of F_N [14], [16]-[17]. It can be shown [9] that for our choice of wing shape, assuming that the air density is 1.28 (kg/m^3), this estimate is equal to:

$$F_N = 0.2038\ R_W^4\ \sin(\alpha_r)\ \dot{\phi}\ |\dot{\phi}| \tag{4}$$

R_W is the wingspan and ϕ is the stroke angle of the wing (Fig. 1.b). α_r represents the angle of attack of the wing (AoA) relative to local air flow (u_r) as illustrated in Fig. 1.a. In our simulations, there are no external air currents and the MAV does not move at very high velocities. Therefore, α_r can be replaced with $\pi/2-\psi$ (Fig. 1.a). We will assume that ϕ has a sinusoidal waveform. Solving (1) to (4) together, it can be seen that with the proposed approach, the wing smoothly rotates and changes direction throughout each half-stroke. Fig. 2.a shows how ψ changes when ϕ is a sinusoid of magnitude 35° at 100 Hz. Note that in this case, the set point of the spring (ψ_0) is set to 0°.

Lift (F_L) drag forces (F_D) are defined as illustrated in Fig. 1. For the case shown in Fig. 2.a, these components are illustrated in Fig. 2.b. As it can be seen, F_D is odd-symmetric during each stroke cycle which results in an average value of zero. Therefore, the overall roll and yaw torques produced by both wings during a single symmetric stroke cycle will be insignificant. This makes steering and maneuverability major challenges in control of an FWMAV. One obvious solution to this problem is to achieve roll torques by flapping the left and right wings at different magnitudes. Since the stroke velocity scales linearly with magnitude, from (1), doing so will result in one side generating a larger force (lift), causing the vehicle to roll towards the other side. The downside to this approach however, is the fact that levitation is now coupled

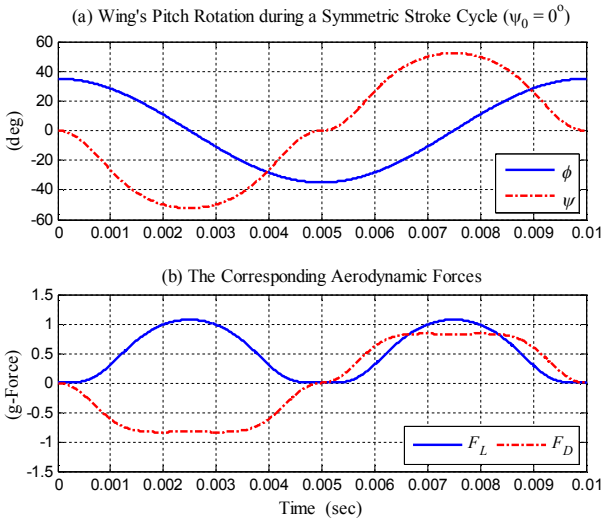

Fig. 2. (a) Evolution of the wing's pitch rotation angle during a symmetric stroke cycle (τ_{ss} = 1). (b) The corresponding aerodynamic forces. In this case, ψ_0 is set to 0°.

with steering, which calls for a more complicated controller to achieve both at the same time.

A more direct method of steering is to use an asymmetric waveform for the stroke angle ϕ, which in turn results in asymmetric aerodynamic forces. For instance, we can change the upstroke-to-downstroke duration ratio, shown by τ_{ss}. Fig. 3.a shows an example for this case. The stroke angle used here is similar to that of Fig. 2.a except τ_{ss} is now changed from 1 to 1.5. The resulting drag profile is asymmetric (Fig. 3.b), and thus, has a nonzero average value which can be used to perform various maneuvers.

This method seems to have been first used by Schenato et al [18], who assumed a saw-tooth waveform for the stroke cycle of the wing. More recently, a sinusoidal version of this asymmetric stroke cycle approach – or split cycle – has been proposed by Doman & Oppenheimer [2] as a method to

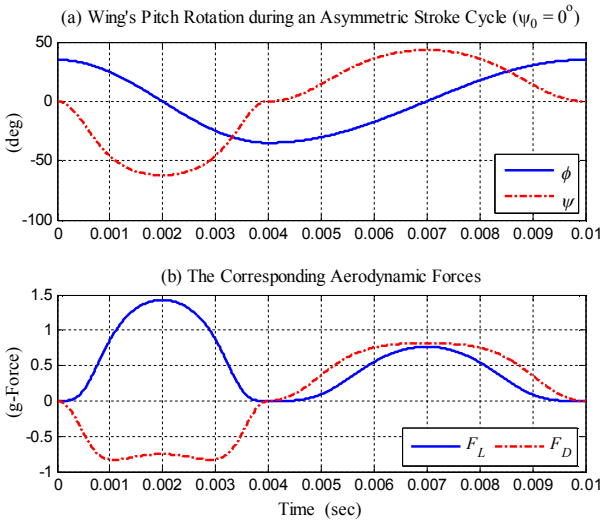

Fig. 3. (a) Evolution of the wing's pitch rotation angle during an asymmetric stroke cycle (τ_{ss} = 1.5). (b) The corresponding aerodynamic forces. In this case, ψ_0 is set to 0°.

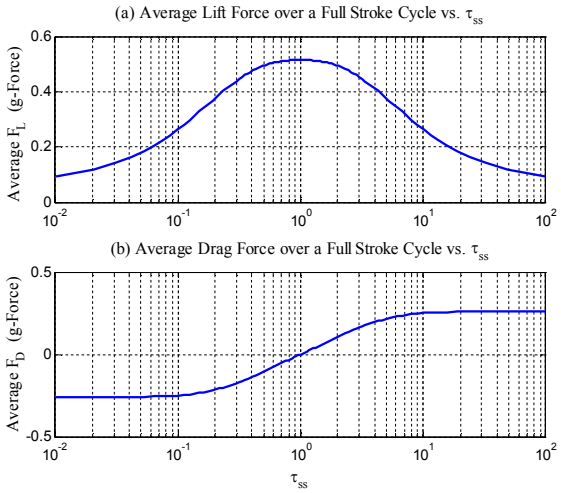

Fig. 4. For a single stroke cycle with magnitude of 35˚ at 100 Hz, the average aerodynamic force is calculated over a wide range of values of τ_{ss}. (a) The net lift force decreases as τ_{ss} changes from 1 while (b) the net drag force increases in magnitude. In these simulations, ψ_0 is set to 0˚.

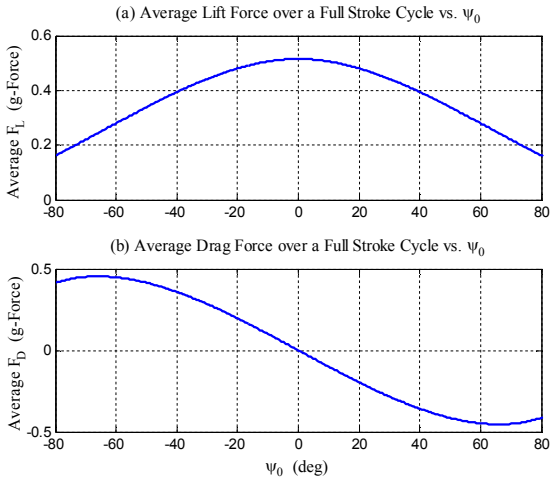

Fig. 6. For a single symmetric stroke cycle (i.e. $\tau_{ss} = 1$) with magnitude of 35˚ at 100 Hz, the average aerodynamic force is calculated as impedance set point ψ_0 is changed. (a) The net lift force decreases as ψ_0 changes from 0˚ while (b) the net drag force increases in magnitude.

control the orientation of an FWMAV. It is important to note that for limited amounts of change in τ_{ss}, i.e. between 0.5 and 2, the average lift force remains almost constant while the average drag force varies over a considerable range (see Fig. 4). Therefore, in this range of operation, levitation and steering are decoupled and can be controlled almost independently. However, in spite of this beneficial advantage, the split cycle method has the disadvantage of operating at frequencies higher than nominal flapping frequency. This calls for stroke actuators with high bandwidth requirements, which complicates the design problem in terms of power and weight limitations.

As a third solution to steering problem, we have proposed a method based on controlling the spring set point ψ_0 [3]. A nonzero set point introduces a phase shift in pitch rotation of the wing with respect to its stroke profile. Thus, even for a sinusoidal stroke angle ϕ with $\tau_{ss} = 1$, the resulting pitch profile ψ is asymmetric (see Fig. 5.a).

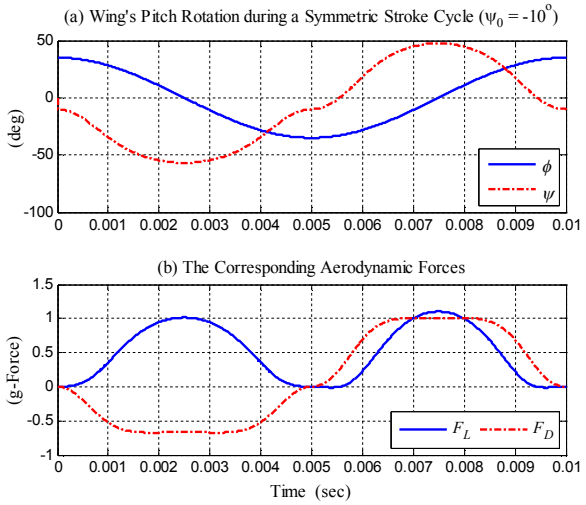

Fig. 5. (a) Evolution of the wing's pitch rotation angle during a symmetric stroke cycle (i.e. $\tau_{ss} = 1$) with impedance set point ψ_0 set to -10˚. (b) The corresponding aerodynamic forces.

Correspondingly, the angle of attack will change differently during upstroke compared to that of downstroke, resulting in an asymmetry in the drag force as illustrated in Fig. 5.b. Similar to the split cycle method, for small values of ψ_0, i.e. between -15˚ and 15˚, the average lift force remains almost constant while the average drag force reaches a considerable nonzero value (see Fig. 6) which indicates that levitation and steering can be decoupled. In addition, a comparison between Fig. 4 and 6 reveals that our proposed method achieves a larger average drag over the decoupling range of its swept parameter. Therefore, we expect higher maneuverability from an FWMAV that uses ψ_0 as the control parameter for steering and horizontal motion.

III. Modeling

The dynamic model of the MAV used in system simulations will be discussed next. A free-body diagram of the system is shown in Fig. 7.

By applying the Newton's equations of motion in the vehicle's body frame, a six degree of freedom dynamic model is derived [3], [19]:

$$m\ (\dot{\vec{v}} + \vec{\omega} \times \vec{v}) = \Sigma \vec{F} \tag{5}$$

$$J\ \dot{\vec{\omega}} + \vec{\omega} \times J\vec{\omega} = \Sigma \vec{M} \tag{6}$$

Vectors v and ω represent the translational and angular velocities of the body. m and J are body mass and body inertia matrix, respectively. The body shape in Fig. 7 is chosen since its corresponding inertia matrix has insignificant nondiagonal terms and therefore, can be assumed to be diagonal. Forces (F) and moments (M) on the body have the following components along each body axis:

$$F_x = F_{D,r,x} + F_{D,l,x} - m\ g_x - b_v\ v_x\ |v_x| \tag{7}$$

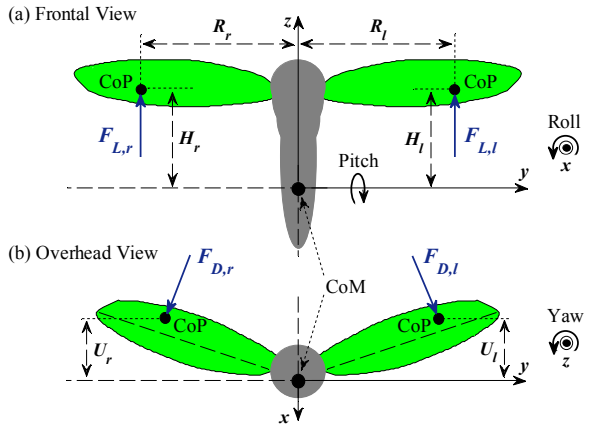

Fig. 7. Free-body diagram of a FWMAV: (a) frontal and (b) overhead view. R, H and U specify the location of center of pressure (CoP) of each wing with respect to the center of mass (CoM) of the whole system. Indices l and r represent left and right, respectively. For simulation purposes, Euler angles in the Tait-Bryan ZXY convention are used to update the orientation of the body.

$$F_y = F_{D,r,y} + F_{D,l,y} - m\ g_y - b_v\ v_y\ |v_y| \tag{8}$$

$$F_z = F_{L,r} + F_{L,l} - m\ g_z - b_v\ v_z\ |v_z| \tag{9}$$

$$M_x = F_{L,r}\ R_r - F_{L,l}\ R_l - F_{D,r,y}\ H_r - F_{D,l,y}\ H_l - b_\omega\ \omega_x \tag{10}$$

$$M_y = F_{D,r,x}\ H_r + F_{D,l,x}\ H_l - F_{L,r}\ U_r - F_{L,l}\ U_l - b_\omega\ \omega_y \tag{11}$$

$$M_z = F_{D,r,y}\ U_r + F_{D,l,y}\ U_l - F_{D,r,x}\ R_r + F_{D,l,x}\ R_l - b_\omega\ \omega_z \tag{12}$$

where indices r and l refer to right and left wings, respectively. The vector $\vec{G} = [g_x, g_y, g_z]$ expresses gravity in the body coordinate frame. The variable b_v is the coefficient of viscous friction and b_ω represents the passive damping while rotating around any of the three body axes, as discussed in [20]. R, H and U represent the distance from center of mass (CoM) of the whole system to the center of pressure of each wing, as shown in Fig. 7. The values used for parameters in (5)-(12) are listed in Table I.

IV. Controller

In this work, we will compare the performance of our proposed approach with that of split cycle method when both are used to control a modeled FWMAV for the purpose of steering. Both methods are based on the idea of creating asymmetry in the profile of drag force during each stroke cycle without causing significant change in the average lift force. The split cycle method (SC) changes τ_{ss}, i.e. it creates asymmetry in the stroke angle profile and thus, indirectly creates asymmetry in the wing's pitch rotation angle ψ (Fig. 3.a). Note that in this case, the impedance parameter ψ_0 remains constant, i.e. 0°. In our approach, which we refer to as tunable impedance (TI), τ_{ss} remains equal to 1 while ψ_0 is varied to create asymmetry directly in the waveform of ψ. As it was observed earlier, an asymmetric profile for ψ will lead to asymmetry in the profile of drag force. Fig. 8 illustrates a general diagram of the controller structure used for each wing. The underlying modules are introduced next.

TABLE I
Physical Properties of the Modeled FWMAV

Symbol	Description	Value
m_{body}	total mass	7×10^{-5} kg
J_{body}	inertia matrix (a 3×3 scalar matrix)	3×10^{-8} N.m.s^2
R_w	length of wing chord	1.5×10^{-2} m
z_{CoP}	distance of CoP of each wing from its pitch rotation axis	1.009×10^{-3} m
b_ω	passive damping coefficient of the body (rotation in either direction)	3×10^{-6} N.m.s
b_v	coefficient of viscous friction along either direction	1×10^{-4} N.s^2/m^2
$H(\psi=0^\circ)$	distance of CoP from transverse plane of the body (xy) when $\psi=0^\circ$	5.42×10^{-3} m
$R(\phi=0^\circ)$	distance of CoP from sagittal plane of the body (xz) when $\phi=0^\circ$	1.191×10^{-2} m
W_{body}	body width at the root of wings	2.16×10^{-3} m
$U(\phi=0^\circ)$	distance of CoP from coronal plane of the body (yz) when $\phi=0^\circ$	1.08×10^{-3} m

A. Altitude Controller

In both methods, the relatively constant average lift force over the allowed range of control variable enables us to control vertical motion independently through adjustment of the stroke's magnitude. A hybrid controller is used to achieve this. For a change in altitude, a proportional sub-controller with height feedback is responsible to stabilize the average vertical velocity (V_V). Upon reaching the vicinity of the target altitude, a PID sub-controller takes charge to stabilize the vertical position. Note that all controllers introduced in this section are implemented in discrete-time with a sampling rate of 100 Hz, i.e. the stroke frequency.

B. Steering/Horizontal Motion Controller

The structure of steering/planar motion controller in both

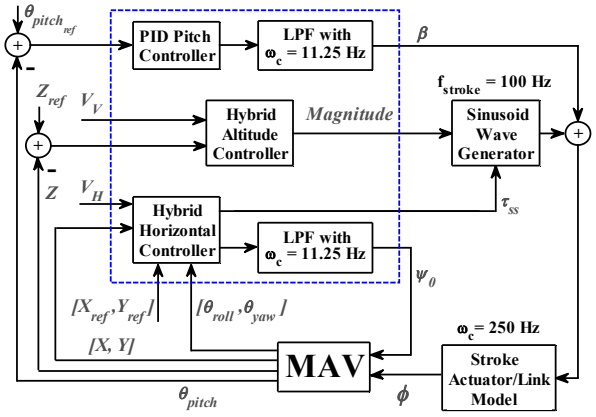

Fig. 8. Block diagram of the flapping-wing MAV's controller system. Crossover frequency of each filter/actuator is represented by ω_c.

methods is similar. However, depending on the method, only one of the parameters τ_{ss} or ψ_0 is changed while the other one remains constant at its nominal value. Remember that τ_{ss} determines the degree of asymmetry in the stroke profile of each wing, e.g., $\tau_{ss}=1$ corresponds to a symmetric waveform. The values of both parameters are limited to suitable ranges that are chosen from Fig. 4 and Fig. 6.

In the case of steering, the value of corresponding control parameter is set to be proportional to the steering deviation from projection of the target on the horizontal plane. To achieve opposing drag forces on the wings, the control parameters on both sides are adjusted in opposite directions. As it will be shown in the results section, while this controller is active, roll angle remains small and can be easily negated by small adjustments in the magnitude of stroke angles – with no significant effect on altitude control. Once the steering deviation is sufficiently small, the planar motion controller is activated. In this case, a hybrid controller similar to the one responsible for vertical motion control is used to adjust the average horizontal velocity (V_H) and stabilize the MAV. Note that when the control parameters of both wings have the same value, the resulting drag forces are equal and in the same direction. Therefore, forward/backward motions become possible.

C. Pitch Controller

From Fig. 7, note that we deliberately consider the more challenging but realistic case of a CoM that is not directly below the average position of center of lift (CoL); such a situation may be a result of carrying variable payloads on any given mission. In this situation, the lift force tends to produce a large pitch torque, making it more difficult to stabilize the MAV. To solve this problem, a PID controller adjusts a bias angel β based on the difference of actual pitch angle from a usually small reference value. This bias angle is added to the stroke angle profile of each wing. The new waveforms are then fed to an actuator model to simulate the actual stroke angles in a real system. These final waveforms along with values of ψ_0 for each wing are used to calculate aerodynamic forces and simulate motion in each stroke cycle.

V. Results

Reasonable values are chosen for gains in each controller through a separate set of tuning simulations [3]. In all experiments, the flapping frequency is set to 100 Hz and the magnitude of the stroke angle may vary between 17.5˚ and 70˚. The nominal stroke magnitude is set to 35˚ in order to maintain enough lift for the MAV to remain levitated. The bias added to the stroke angle is always less than 15˚ in magnitude. As for steering/planar motion control, the acceptable ranges for control parameters are chosen by looking at Fig. 4 and 6. Thus, τ_{ss} is bounded between 0.5 and 2 (i.e., between 33% and 67% of a cycle is spent in the upstroke, with the remainder in the downstroke) while ψ_0 can have any value between −15˚ and 15˚. For simulation purposes, Euler angles in the Tait-Bryan ZXY convention are used to update the orientation of the body.

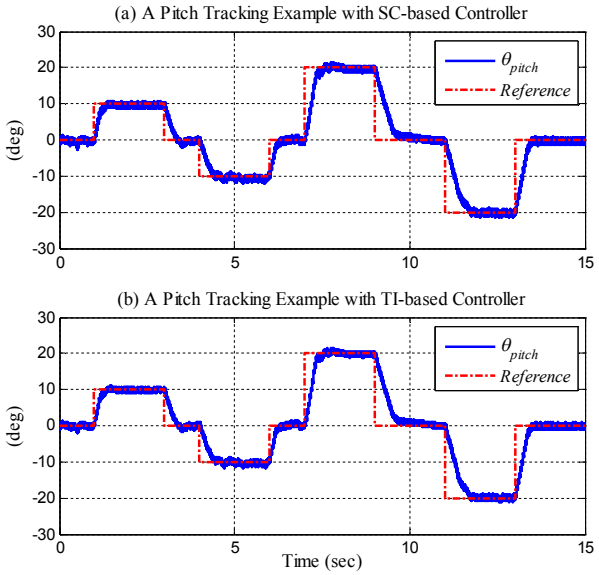

Fig. 9. Pitch response of the model to an arbitrary reference signal with (a) SC and (b) TI-based controllers. Gaussian white noise with standard deviation of 0.5˚ is added to the feedback pitch angle to simulate measurement noise.

A. Pitch/Yaw Tracking

To test the maneuverability of the system, we have to examine how well each controller can track pitch and yaw reference commands. As a first experiment, we force each controller to track the same reference pitch command (Fig. 9) while hovering. Gaussian white noise with standard deviation of 0.5˚ is added to the feedback pitch angle to simulate measurement noise. The actual pitch angles are also plotted. In both cases, the system is able to quickly track sudden changes in the reference pitch angle. Note that the responses in Fig. 9.a and Fig. 9.b are very similar. This is partially due to the fact that both methods are using the same pitch control mechanism. Furthermore, since the vehicle is in hovering mode, the required force adjustments will be very small and their influence on pitch angle of the body will be insignificant.

A similar set of experiments are designed to examine and compare the steering capabilities of both approaches. These simulated experiments are performed in hovering mode while pitch angle is kept as small as possible; making the Eulerian yaw angle a good approximation of the model's true heading in global coordinates. Fig. 10 shows the performance of each method while tracking the same reference yaw command. A Gaussian white noise with standard deviation of 0.5˚ has been considered in this case, too. Both methods are capable of reorienting the model in the desired direction. Note that reorientation happens

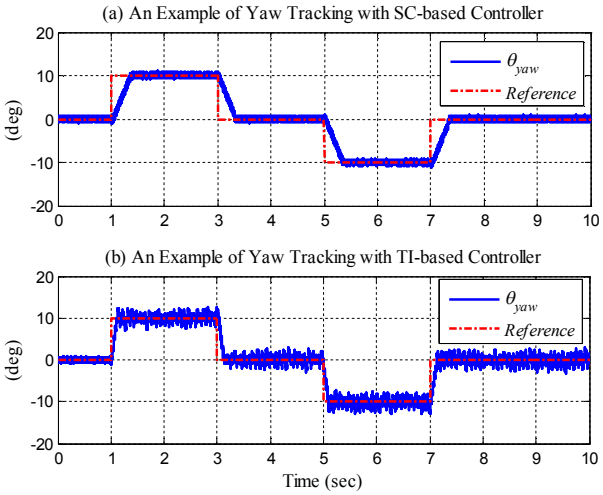

Fig. 10. Yaw response of the model to an arbitrary reference signal with (a) SC and (b) TI-based controllers. Gaussian white noise with standard deviation of 0.5˚ is added to the feedback yaw angle to simulate measurement noise.

relatively faster when TI-based controller is used.

B. Steering and Horizontal Motion

In our most informative experiments, the model is expected to reach a specified target position [X_{ref}, Y_{ref}, Z_{ref}], starting from hovering condition. Target is placed in various locations with respect to the initial position of the model. Depending on the location of the target, the MAV may need to reorient or move forward/backward. Furthermore, the target may be in a different altitude than what the model is initially at, and thus, altitude adjustment may also be required. Each trial is repeated for the model with both types of steering/planar motion controllers described in section IV. In both cases, Gaussian white noises with standard deviations of 0.5˚ and 1 mm are respectively added to the feedback angles and position components to simulate measurement noise.

The initial distance of the target varies between 0.5 m and 1 m, however, the MAV is always able to reach the target in a few seconds without becoming unstable. Results of a sample trial with SC and TI-based controllers are shown in Fig. 11 and Fig. 12, respectively (X_{ref}= Y_{ref}= Z_{ref} = 0.5 m). By comparing the two diagrams, we see that steering with TI-based controller is relatively faster. This is not unexpected, since the maximum average drag force generated over the allowed range of ψ_0 is about 1.5 times of what can be achieved in case of adjusting τ_{ss} (compare Fig. 4.b and Fig. 6.b).

As a second advantage, we note that steering with SC-based controller is accompanied with significant undesired translational motion which will be much less when using the other controller (Fig. 13). Thus, TI method provides us with the capability of in place rotation, a maneuver that is particularly useful for obstacle avoidance in crowded or narrow environments.

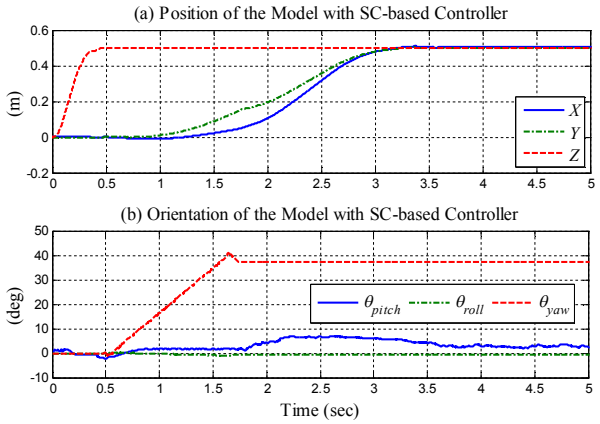

Fig. 11. A sample trial of movement towards a target experiment when using the SC-based controller in presence of measurement noise. Evolution of (a) position and (b) orientation of the modeled flapping-wing MAV.

VI. Conclusion and Future Work

In this paper, our main focus is on the issue of steering and motion control of microrobotic insects while moving in the horizontal plane. We argued that in contrast to traditional approach of choosing different stroke magnitudes for each wing, a better method is to create appropriate asymmetries in the drag profile of both wings. A known example of the latter is the "split cycle" method, which is based on adjusting the upstroke-to-downstroke duration ratio.

The traditional approach relies mainly on roll torques that are created by the difference between lift forces of both wings. This means that steering maneuvers will affect the levitation of the vehicle. On the other hand, steering in methods such as "split cycle" is based on roll/yaw torques that are produced by the now non-zero average drag force of each wing. Depending on the control parameter, we can find a limited range in which, significant values of average drag force are accompanied with none or little change in the value of average lift force. This allows us to control steering and levitation independently, using simple strategies such

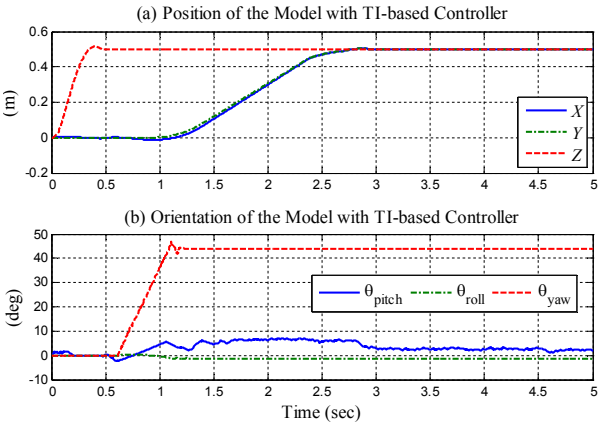

Fig. 12. A sample trial of movement towards a target experiment when using the TI-based controller in presence of measurement noise. Evolution of (a) position and (b) orientation of the modeled flapping-wing MAV.

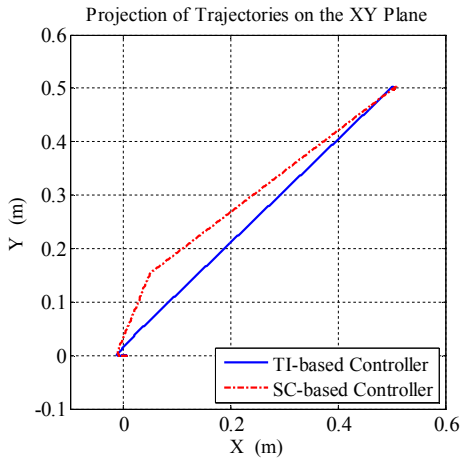

Fig. 13. Projection of trajectories in Fig. 11.a and Fig. 12.a on the horizontal plane. In comparison with TI method, the model with SC-based controller moves significantly while steering towards the target.

as PID control.

The "split cycle" method changes the shape of stroke profile for both wings which results in performing either upstroke or downstroke at a frequency higher than 100 Hz. Therefore, each wing requires a separate stroke actuator with a bandwidth larger than the actual frequency of flapping.

Here, we introduced a new motion control method based on a "tunable" passively rotating wing design. The idea is to create an offset in the wings' pitch rotation angles by adjusting the impedance parameters and thereby, creating asymmetries in the drag profile of each wing. This allows us to use the same symmetric stroke profile for both wings, i.e. a single stroke actuator can now drive both of them. Note that this actuator requires a bandwidth only as high as the frequency of flapping, i.e. 100 HZ. The necessary impedance actuators operate at a much slower pace [3] and therefore, require a low bandwidth. Furthermore, low-powered actuators such as [13] can be used for this purpose which will significantly reduce the weight of the on-board battery and facilitate the design problem.

We have compared the performance of our method to that of a split cycle method through a set of simulated experiments. The results show that our method is both faster and capable of smoother motion control. This is mainly due to the fact that within our decoupling range of control parameter, greater values of average drag force are achievable. In addition, the resulting step responses for body angle show that if the reference pitch angle does not change too drastically (e.g., step increases of less than 20˚), the model is easily able to stabilize near the new, desired pitch angle. Our method also demonstrates accurate yaw tracking maneuvers even in presence of measurement noise.

In our future work, we plan to implement this method on a 3-inch-wingspan FWMAV. We intend to merge this method with a suitable trajectory tracking and navigation algorithm in order to test the vehicle in field experiments. Improving the controllers is another issue we plan to address in the near future.

Our method relies heavily on sensory input which is a main challenge in design of FWMAVs. Incorporating internal models as done in [21] is an interesting approach to reduce this reliance. However, the nonlinear nature of flapping systems may result in complex internal models, especially in case of body angles. The existence of such models and their degree of complexity is another area that remains open for further investigation.

REFERENCES

[1] R. J. Wood, "The first takeoff of a biologically inspired at-scale robotic insect," *IEEE Transactions on Robotics*, 24:341–347, 2008.

[2] D. B. Doman, and M. W. Oppenheimer, "Dynamics and control of a minimally actuated biomimetic vehicle: part I. aerodynamic model," AIAA Guidance, Navigation, and Control Conference, San Francisco, California, USA, 10-13 August, 2009.

[3] H. Mahjoubi, and K. Byl, "Analysis of a tunable impedance method for practical control of insect-inspired flapping-wing MAVs," 2011 50th IEEE Conference on Decision and Control and European Control Conferene (CDC-ECC), Orlando, FL, USA, December 12-15, 2011.

[4] T. McGeer. "Passive dynamic walking," The International Journal of Robotics Research, 9(2): 62–82, 1990.

[5] S. H. Collins, A. Ruina, R. Tedrake and M. Wisse, "Efficient bipedal robots based on passive-dynamic walkers," Science, 307: 1082–1085, 2005.

[6] A. Goswami, B. Espiau, and A. Keramane, "Limit cycles and their stability in a passive bipedal gait," IEEE International Conference on Robotics and Automation *(ICRA)*, pp. 246–251, 1996.

[7] P. S. Sreetharan and R. J. Wood, "Passive torque regulation in an underactuated flapping wing robotic insect," Robotics: Science and Systems, Zaragoza, Spain, June 2010.

[8] A. J. Bergou, S. Xu and Z. J. Wang, "Passive wing pitch reversal in insect flight". J. Fluid Mech., 591, pp. 321–337, 2007.

[9] K. Byl, "A passive dynamic approach for flapping-wing micro-aerial vehicle control," ASME Dynamic Systems and Control Conference, Cambridge, Massachusetts, USA, 13-15 September 2010, 2010.

[10] R. K. Josephson, "Chapter 3: Comparative Physiology of Insect Flight Muscle," in Nature's Versatile Engine: Insect Flight Muscle Inside and Out. (Vigoreaux and Josephson, ed.) pp. 34-43, Springer US, 2006.

[11] R. Dudley, *The Biomechanics of Insect Flight: Form, Function, Evolution*. Princeton University Press, 2000.

[12] G. K. Taylor, "Mechanics and aerodynamics of insect flight control," Biol. Rev., 76, pp. 449–471, 2001.

[13] T. Miura, T. Shirai, and T. Tomioka, "Proposal of joint stiffness adjustment mechanism SAT," JSME Conference on Robotics and Mechatronics '02, pp. 29, 2002. (in Japanese)

[14] C. P. Ellington, "The aerodynamics of hovering insect flight I. the quasi-steady analysis," Philosophical Transactions of the Royal Society of London, 305(1122), pp. 1-15, 1984.

[15] M. F. M. Osborne, "Aerodynamics of flapping flight with application to insects," Journal of Experimental Biology, 28(2), pp. 221-245, 1951.

[16] S. P. Sane, and M. H. Dickinson, "The control of flight by a flapping wing: lift and drag production," Journal of Experimental Biology, 204, pp. 2607-2626, 2001.

[17] W. B. Dickson, and M. H. Dickinson, "The effect of advance ratio on the aerodynamics of revolving wings," Journal of Experimental Biology, 207, pp. 4269-4281, 2004.

[18] L. Schenato, D. Campolo, and S. Sastry, "Controllability issues in flapping flight for biomimetic micro aerial vehicles (MAVs)". IEEE International Conference on Decision and Control, Dec., 2003.

[19] X. Deng, L. Schenato, W. C. Wu, and S. S. Sastry, "Flapping flight for biomimetic robotic insects: part I–system modeling," *IEEE Transactions on Robotics*, 22(4), pp. 776–788, 2006.

[20] T. L. Hedrick, B. Cheng, and X. Deng, "Wingbeat time and the scaling of passive rotational damping in flapping flight," Science, 324, 2009.

[21] N. O. Perez-Arancibia, J. P. Whitney, and R. J. Wood, "Lift force control of flapping-wing microrobots," to appear: *IEEE transactions on Mechatronics*, 2011.